The effects of silver nanoparticle shape on protein adsorption and neural stem cell viability

Murali Kumarasamy (drmuralinano@gmail.com)
Hungarian Academy of Sciences Institute of Experimental Medicine: Magyar Tudomanyos Akademia Kiserleti Orvostudomanyi Kutatointezet https://orcid.org/0000-0002-8946-5423

Ngoc Tran
Ho Chi Minh City University of Natural Sciences: Truong Dai hoc Khoa hoc Tu nhien Dai hoc Quoc gia Thanh pho Ho Chi Minh

Javier Patarroyo
Catalan Institute of Nanoscience and Nanotechnology: Institut Catala de Nanociencia i Nanotecnologia

Marco P Monopoli
Royal College of Surgeons in Ireland

Emilia Madarasz
Hungarian Academy of Sciences Institute of Experimental Medicine: Magyar Tudomanyos Akademia Kiserleti Orvostudomanyi Kutatointezet

Víctor F Puntes
Catalan Institute of Nanoscience and Nanotechnology: Institut Catala de Nanociencia i Nanotecnologia

Research Article

Keywords: Silver nanoparticles, geometries, cellular uptake, neurotoxicity, neural stem cells, protein corona

Posted Date: March 22nd, 2021

DOI: https://doi.org/10.21203/rs.3.rs-303756/v1

Abstract

Silver nanoparticles (AgNPs) are important and widely used antimicrobials and nanodrug carriers. The increased use of AgNPs in consumer products has raised concerns about nanosafety; for instance, AgNPs may be inhaled and translocate to the brain via olfactory neural stem cells/progenitors. While the biological effects of nanoparticle size have been widely investigated, there are little data on the effects of particle shape on cellular phenotype. Therefore, here we investigated the interactions between AgNP spheres, rods, cubes, and triangles and human plasma proteins and their effects on the viability of NE-4C neural stem cells. Nanoparticles were synthesized by wet chemistry methods and characterized by UV-vis spectroscopy, dynamic light scattering, zeta potential measurement, transmission electron microscopy, nanoparticle tracking analysis, and differential centrifugal sedimentation. NE-4C cell viability was assessed using the MTT reduction assay, and the cellular uptake of differently shaped nanoparticles was monitored by electron microscopy. All 50 nm (in at least one dimension) AgNPs exerted toxic effects, with rods and cubes displaying greater toxicity than spheres and triangles. These cellular and physicochemical results indicate that edges on the AgNPs increase toxicity, presumably due to enhanced ion dissolution from the edges.

Introduction

Silver nanoparticles (AgNPs) are widely used in a variety of commercial applications including electronics, paints, clothing, food, cosmetics, and medical devices due to their desirable catalytic, optic, magnetic, and antibacterial properties. According to the Woodrow Wilson database, about 50% of all consumer products are thought to contain engineered nanosilver [1]. As a consequence of this widespread use, humans are potentially exposed to AgNPs through the dermal, oral, or inhalation routes. AgNPs can be inhaled during their manufacture or their subsequent use, such as when used as aerosol disinfectants or as over-the-counter homeopathic sprays for the treatment of respiratory infections [2–5]. By virtue of their small size, AgNPs can easily penetrate into the lower respiratory tract, which, through its specialization for gaseous exchange with the circulation, possesses an immense surface area for their deposition and systemic transport.

However, AgNPs have also been shown to have effects on the central nervous system [6]. They can enter the nasal cavity and translocate to the brain via the olfactory epithelium, which directly connects the nose and the brain [5–9]. In particular, animal modeling has shown that some nanomaterials can translocate to the brain to affect its function [10–12]. Nanoparticles, viruses, and other molecules can bypass the blood-brain barrier (BBB) and be transported from the olfactory epithelium in the nasal cavity to the olfactory bulb in the forebrain [7, 10, 13] via three potential pathways: a) transcellular transport across sustentacular cells of the olfactory epithelium; b) paracellular transport through junctions in the olfactory epithelium; or c) intracellular transport through axonal movement via olfactory nerve fascicles to the synaptic junctions within the OB [13]. Nanoparticle translocation along olfactory nerve fascicles and accumulation in the OB have been particularly well studied [5, 7, 14–19].

Mechanistically, AgNPs have been shown to dysregulate a number of different cell types and signaling pathways both *in vitro* and *in vivo*. AgNPs introduced into the systemic circulation can induce BBB dysfunction, astrocyte swelling, and neuronal degeneration [20, 21]. AgNPs have been shown to block the vascular endothelial growth factor (VEGF)-induced proliferation and migration of bovine retinal endothelial cells (BRECs) and induce apoptosis [22]. AgNPs have been shown to increase the membrane permeability of primary rat brain endothelial cells by activating proinflammatory mediators [23]. 20 nm AgNPs were found to activate rat lung epithelial (RLE) and rat aortic endothelial (RAEC) cells in an interleukin-6 (IL-6)-dependent manner [24]. Furthermore, AgNPs but not Ag^+ ions have been shown to induce inflammatory signaling pathways [25, 26]. Clathrin-mediated endocytotic uptake and cytoplasmic and nuclear accumulation of AgNPs have been observed in U251 human glioblastoma cells [27, 28], and AgNPs have been shown to accumulate in primary astrocytes in a concentration-dependent manner [29]. 20 and 80 nm AgNPs affected the growth of human embryonic neural precursor cells [30], and all retinal neuronal layers took up the particles and displayed neural damage [30]. Finally, AgNPs have been shown to affect neurite outgrowth and reduce the viability of premature neurons and glial cells [31, 32]. Recent studies have also demonstrated that the geometries of NPs impact protein corona formation [33], circulation time, cellular uptake, and bio-distribution [34]. In the last few years, we conducted systematic *in vitro* 2-dimensional [35–37] and 3-dimensional (brain organoids and spheroids) [38, 39] studies to evaluate cellular neurosafety and neural uptake of well-characterized polymeric, metallic (Ag and Au) and ceramic NPs. Among various physico-chemical properties known to influence biological activities, In this study we focused on the different shape of Ag NPs. There is a growing body of evidence that AgNPs can have adverse effects on the central nervous system. However, there have been few studies of the effects of different shapes of AgNP on neural cell function. Since the growth, shape, and size of AgNPs can easily be modified using polyvinylpyrrolidone (PVP) as a structure-directing polymer [40–42], here we investigated the synthesis and cellular effects of different shapes of AgNP on NE-4C neural stem cells.

Materials And Methods

Preparation of silver (Ag) NPs

50 nm bare and PVP-coated AgNPs were synthesized according to Bastús and co-workers [43]. 1 ml of 0.5 M sodium citrate and 1 ml of 25 mM tannic acid were mixed with 97 mL H_2O in a three-neck round-bottomed flask. The mixture was heated to boiling with vigorous stirring followed by fast injection of 1 ml 50 mM $AgNO_3$. NP growth was achieved by consecutive addition of 50 mM $AgNO_3$ (1 ml per addition). After each injection, the solution was kept under reflux to complete the reaction for 30 mins. 50 nm spherical AgNPs were obtained at the 10th injection. The as-prepared NPs were centrifuged at 8000 x g for 15 min prior to conjugation with PVP.

Conjugation of silver nanoparticles with polyvinylpyrrolidone

Synthesized AgNPs (~50 nm, 7.5×10^{11} NPs/mL) were redispersed in a fresh solution of 5 mM polyvinylpyrrolidone (PVP, MW = 55 kDa) and vigorously stirred for 72 h. Then, the AgNPs were washed again to eliminate excess PVP.

Synthesis of Ag nanocubes

Ag nanocubes were synthesized as in [44]. Briefly, ethylene glycol (5 ml; EG) was heated with magnetic stirring in a 100 ml round-bottomed flask in an at 150°C. Sodium hydrosulfide (NaSH; 0.06 ml; 3 mM in EG) was quickly injected into the solution after its temperature reached 150°C. After 2 min incubation, 0.5 ml aliquots of 3 mM HCl in EG and then 1.25 ml PVP (20 mg/ml in EG, MW 360 kDa) were injected into the reaction solution. After another 2 min incubation, silver trifluoroacetate (CF_3COOAg; 0.4 ml, 282 mM in EG) was added into the mixture. During the entire process, the flask was capped with a glass stopper except when adding reagents. After addition of CF_3COOAg, the transparent solution became a whitish color and then slightly yellow after 1 min, indicating the formation of Ag seeds and then nanocubes.

Synthesis of PVP-coated Ag nanotriangles

PVP-coated Ag nanotriangles were synthesized as in [45]. A 24.04 mL aqueous solution containing $AgNO_3$ (0.05 M, 50 µL), trisodium citrate (75 mM, 0.5 mL), PVP (40K, 17.5 mM, 0.1 mL), and hydrogen peroxide (H_2O_2; 30 wt%, 60 µL) was vigorously stirred at room temperature in air. Sodium borohydride ($NaBH_4$, 100 mM, 250 µL) was rapidly injected into this mixture to initiate the reduction. The solution gradually turned from light yellow to dark blue within 60 mins.

Synthesis of Ag nanorods

0.5 ml of $FeCl_3$ solution (0.6 mM, in EG) was added to 6 ml EG in a round-bottom flask and was heated to 150 ± 4°C. Then, 6 ml EG solution containing 0.052 M $AgNO_3$ and 0.067 M PVP (average molecular weight 360 kDa) was added. The reaction mixture was kept at 150 ± 2°C with stirring at 250 rpm until $AgNO_3$ was completely reduced (about 70–90 minutes).

To examine the yield and morphology of Ag nanorods, 1 ml of the resulting suspension was diluted with 8 ml acetone and 8 ml ethanol and centrifuged at 2000 rpm for 10 min twice. At every stage, the supernatant solution was measured with a UV spectrometer to confirm the relative amount of AgNPs. All the synthesized AgNPs were washed several times with water and then stored at 2–8°C and protected from light.

Transmission electron microscopy (TEM)

TEM images were obtained with a JEOL JEM 1010 (JEOL Ltd., Tokyo, Japan) and Phillips CM20 (Philips, Amsterdam, Netherlands) at 200 keV using carbon grids (S162, Plano GmbH, Wetzlar, Germany). Carbon grids were dried at room temperature (RT), and the areas of the grid were observed at different magnifications. TEM pictures were computer analyzed *in situ* and the size distribution and average size of particles were determined.

Dynamic light scattering (DLS) and Z-potential measurement

NPs suspended in water, phosphate buffered saline (PBS), 10% fetal calf serum in PBS, and culture medium were characterized by dynamic light scattering (DLS) and by zeta-potential determination (Malvern Zetasizer Nano ZS90; Malvern, UK). Particles were sonicated for approximately 20 seconds

before being dispersed in the appropriate dispersants. All DLS measurements were performed with a Malvern Zetasizer Nano ZS90 (Malvern) operating at a light source wavelength of 532 nm and a fixed scattering angle of 173° on 1 ml aliquots of the NP suspensions. Zeta-potential and DLS assays were performed at 25°C and 37°C and are presented as averages and standard deviations of the data obtained from 3 to 5 assays in each solution.

UV–visible spectrophotometry of AgNPs

UV–visible spectra of 1 ml aliquots of the NP suspensions were assayed with a Shimadzu UV-2400 spectrophotometer in the 300–800 nm wavelength range. This technique provides characteristic absorbance maxima for metallic NPs (due to their surface plasmon resonance), which changes with the size, morphology, and surface alterations of the NPs. UV-vis extinction spectra were taken at room temperature using a 1 cm optical path quartz cuvette by diluting 0.1 mL of sample solutions into 1 mL.

Nanoparticle tracking analyses (NTA)

Nanoparticle tracking analyses (NTA) were performed using a Nanosight LM10 (NanoSight Ltd., Salisbury, UK) equipped with a red laser (630 nm) and CCD camera. The samples were dispersed in milli-Q water, and the experiments were performed at 22°C. The Brownian motion of the particles was analyzed on 60-second records by the NTA software.

Differential centrifugal sedimentation (DCS)

DCS experiments were performed with a disc centrifuge (Model DC 24000; CPS Instruments Europe, Oosterhout, The Netherlands). A gradient of 2–8% sucrose equilibrated with spinning at 22,000 rpm for 30 minutes was established and calibrated by running standard polystyrene beads. After establishment of the gradient, 100 μl aliquots of particles dispersed in water were injected. Samples were spun for approximately 2 hours for PS NPs and 5–10 minutes for spherical AgNPs. The position of particles in the gradient was analyzed with CPS software. The tallest peak (the most frequent size value) was regarded as the 'base' peak (100%), and all other particle size peaks were normalized against this base peak (relative size distribution).

Human blood proteins on spherical Ag PVP NPs

In situ protein coronas on spherical Ag PVP NPs were prepared by incubating 0.1 mg/ml NPs in 10%, 80%, and 100% human plasma solution (total protein content 34–47 mg/ml) at room temperature for 1 hour.

The human plasma was obtained from the Centre for BioNano Interactions (CBNI), School of Chemistry and Chemical Biology, University College Dublin, Dublin, Ireland. The blood donation procedure was approved by the Human Research Ethics committee at University College Dublin. The blood plasma was prepared following HUPO BBB SOP guidelines [46]. In brief, after blood collection, the blood was mixed with 2 mM EDTA and centrifuged for ten minutes at 1300 x g at 4°C. Plasma from each donor was collected into 50 ml Falcon tubes and then centrifuged at 2400 x g for 15 minutes at 4°C. The supernatant was collected, aliquoted into 1 ml cryovials, and stored at -80°C until use. Following this procedure, the plasma protein concentration was estimated to be 80 g/l. Before the experiments, the plasma sample was thawed at RT and centrifuged for 3 min at 16,200 RCF. After incubation with human

plasma, the NP samples were directly injected into the DCS instrument without spinning down and washing.

NE-4C neuroectodermal stem cell culture

NE-4C neuroectodermal stem cells (ATTC CRL-2925 [47]) were cloned from primary brain cell cultures prepared from the fore- and midbrain vesicles of 9-day-old transgenic mouse embryos lacking functional p53 tumor suppressor protein. NE-4C neuroectodermal stem cells were maintained in poly-L-lysine-coated culture dishes in minimum essential medium (MEM; Sigma Aldrich, St. Louis, MO) supplemented with 4 mM glutamine and 10% fetal calf serum (FCS; Sigma Aldrich) (MEM-FCS).

Cell exposure to nanoparticles

For viability assays, the cells were grown in 96-well plates (10^4 cells/well) and were exposed to different doses of NPs (from µg/ml;) in serum-free MEM-F12-ITS medium for 24 hours. For uptake experiments, the cells were grown in 24-well plates (10^5 cells/well) and were exposed to 50 µg NPs (10^{10} NPs/ ml) in MEM-F12-ITS medium for 1 h. During exposure to NPs, the cells were kept at 37ºC in a 5% CO_2 and 95% air atmosphere incubator. The NP dispersions were prepared immediately before use and vortexed before distribution in the culture wells.

Cell viability assays (MTT reduction)

For assessing MTT reduction, an index of cellular activity, we used the redox reaction of the same compound 3-(4,5-dimethylthiazol-2-yl)-2,5-diphenyltetrazolium bromide (MTT). MTT can be reduced to a purple formazan [48], and formazan production can be determined by photometrically measuring the absorption of 550–570 nm wavelength light. The metabolic activity of cells was measured by the MTT reduction assay on living cells [48].

Cells grown on 96-well plates (10^4 cells/well) were exposed to NP suspensions (from 7.8 to 250 µg/ml) in 100 µl of MEM-F12-ITS. The cells were incubated for 24 h at 37°C in 95% air and 5% CO_2 atmosphere. The reaction was stopped by adding 100 µl stop solution containing 50% dimethylformamide and 20% sodium dodecyl sulfate in distilled water (DMF-SDS, pH 4.7). After dissolving the cell material and the formazan product in the stop solution, formazan quantity was determined by measuring light absorption at dual [550–570 nm (measuring) and 630–650 nm (reference)] wavelengths using a Bio-Rad 450 (BioRad Hungary Ltd., Budapest, Hungary) or Dynatech MR5000 (Dynatech Industries Inc., McLean, VA). To obtain comparable data on different cells and culture plates, optical density data measured in each well were related to values obtained on control (non-exposed) cells on the same plate (100%). The data were presented as relative percentages of the control. Averages and standard deviations were calculated from 8–12 identically treated cultures. Significance was calculated with the Student *t*-test. Differences were regarded statistically significant if p-values were < 0.05 and biologically significant if dose-dependent responses were detected.

TEM analysis of the cellular uptake of AgNPs of different shape

Neural stem cells were grown on poly-L-lysine-coated glass coverslips in 24 well plates (10^5 cells/well). The cells were incubated with 500 µl suspension of 50 µg/ml (2 x 10^{11} NPs/ml) NPs dispersed in MEM-F12-ITS for 1 h at 37°C in a CO_2 incubator. Control cells were incubated without NPs. The cells were washed three times with PBS (pH 7.4) to remove free-floating NPs and fixed for 20 min with freshly prepared glutaraldehyde 1% and 4% PFA solution before being post fixed in 2% osmium tetroxide (OsO_4) in 0.1 M PBS pH 7.4 at 4°C for 2 hours. After washing, the preparations were dehydrated in increasing (30%, 60%, 96% v/v) concentrations of ethanol and embedded in LX-112 resin (Ladd, Burlington, VT). Sections (60–80 nm) were cut with an ultracut (UCT, Leica EM UC7, Wetzlar, Germany) and then contrasted with 1% uranyl-acetate in 50% ethanol and examined by TEM as above.

Results

Synthesis and physicochemical characterization of differently shaped AgNPs

Cubical, triangular, rod-shaped, and spherical AgNPs were synthesized using the polyol process [49, 50], with polyvinylpyrrolidone (PVP) as the protecting agent and ethylene glycol (EG) as both the reducing agent and solvent. In this synthesis, the reaction temperatures and times as well as the concentration of protective agent are the key parameters controlling the size and geometries of the metal particles [51]. The sphere diameters and edge lengths of nanocubes and triangles, respectively, were 35–55 nm, while the thickness of triangular platelets was ~ 5 nm and the lengths of rods 40–70 nm in cross-sectional diameter reached several micrometers. The different geometries of AgNPs were characterized by transmission electron microscopy (TEM) and UV-vis spectroscopy [52], with the spherical AgNPs also characterized by nanoparticle tracking analysis (NTA) and differential centrifugal sedimentation (DCS). UV-vis spectroscopy exploits the surface plasmon resonance (SPR) of metal nanoparticles to reflect the abundance of edges and sharp points in the particles [52].

Spherical AgNPs were produced at concentrations of 0.1 g/L or 1.5 x 10^{11} NPs/ml. Monodisperse suspensions were stabilized with either sodium citrate or PVP in the solvent. UV-vis spectroscopy (Fig. 1A) revealed the typical optical characteristics of a colloidal suspension of ~ 50 nm spherical AgNPs. The size distribution was determined by NTA (Fig. 1B) and by TEM (Fig. 1C), which indicated 47 ± 3 nm and 47 ± 7.8 nm particle sizes, respectively. The TEM images revealed spherical, mainly isodimensional monodisperse particles (Fig. 1C). Monodispersity was also confirmed by DCS (Fig. 1D). The zeta-potential of the spherical AgNPs was − 20 mV in PVP-stabilized suspensions.

Silver nanocubes were synthesized by reducing silver trifluoroacetate with EG in the presence of PVP. Thirty minutes after the addition of CF_3COOAg, Ag nanocubes with an edge length of 35–40 nm were obtained. Depending on the reaction time, the edge lengths of the Ag nanocubes could be increased up to 70 nm, allowing tuning of their size to between 30 and 50 nm. The synthesis was also optimized by adjusting the reaction temperature up to 153 ± 5°C and by adding PVP (360 kD monomeric unit) to the reaction system. UV-vis spectroscopy (Fig. 2A) showed a characteristic shoulder peak around 350 nm, indicating the presence of silver nanocubes, which was also confirmed by TEM (Fig. 2B).

Silver nanotriangles were prepared by reducing an aqueous silver nitrate solution with $NaBH_4$ in the presence of trisodium citrate, PVP, and hydrogen peroxide (H_2O_2). PVP was used to improve the size distribution of the nanotriangles/plates. While the characteristic sharp shoulder peak around 330 nm can be caused by quadrupole resonance of silver nanotriangles, the long peak shifting towards longer wavelengths indicated the formation of nanotriangles/plates (Fig. 2C), which was also confirmed by TEM (Fig. 2D).

Silver nanorods were characterized by UV-vis spectroscopy (Fig. 2E). The spectrum reflected the anisometric geometry of Ag nanorods, with a sharp absorbance at 350–390 nm, the optical fingerprint of Ag nanorods [53–56]. The formation of silver nanorods was confirmed by TEM (Fig. 2F), and the final concentration of freshly prepared Ag nanorods was 3.8 x 10^9 NPs/ml (1.08 g/L by ICP-MS).

Protein adsorption by AgNPs

We next studied the dispersion of and protein corona formation with AgNPs incubated in human plasma at three concentrations [10, 80, and 100% (v/v in PBS)]. DCS measurements focusing on spherical NPs revealed that AgNP-protein complexes were monodispersed at all three human plasma concentrations (full corona, FC). The main plasma concentration peak shifted to the left, suggesting an increase in protein corona thickness (Fig. 3A). This adsorption of proteins on the NP surface is typical for systems in which the protein density is lower than the NP density. As demonstrated in Fig. 3A, at high plasma concentrations (from 80%), free plasma proteins sometimes aggregated. The Vroman effect [57] predicts that the adsorption of blood serum proteins to inorganic surfaces is time dependent: serum proteins with the highest mobility (or closest to the surface) arrive at the surface first and are gradually replaced by less motile proteins with a higher affinity for the surface; this process may take several hours. To study the effect of different geometries of silver NPs on protein corona formation (Fig. 3B), we incubated the spherical, cubic, triangular, and rod-shaped AgNPs in human plasma for 1 and 24 h with continuous agitation. When AgNPs of different shapes were incubated with 100% human plasma, besides time dependency, the rate of protein adsorption was shape dependent. AgNP consumption and protein corona formation *in situ* revealed that AgNPs with angles and edges adsorbed more proteins than those with a spherical shape after both short and long incubation times (Fig. 3B). These results agree with a previous report that specific proteins such as lysozyme and α-chymotrypsin adsorbed more on metal nanorods compared to nanospheres [58].

The rod-shaped and triangular NPs, where the curvature is only one dimensional (1D), allow for greater protein density and adsorption, since increased lateral interactions on the relatively “flat” cylindrical surface facilitate protein adsorption compared to on spherical NPs [58].

Cellular responses to differently shaped AgNPs

AgNPs are known to be toxic to microbes and tissues, mainly due to the release of Ag^+ ions [59]. We therefore investigated the influence of particle shape on mammalian cellular toxicity. Differently shaped 50 nm AgNPs were incubated with NE-4C embryonic neuroectodermal stem cells for 24 hours at increasing (1–100 mg/ml) concentrations, and the MTT metabolic assay was performed to assess cell

viability. Metabolic activity (i.e., MTT reduction capacity) was reduced below 20% of control by Ag rods at 1 µg/ml and by cubes at 50 µg/ml concentrations (Fig. 4A). Ag triangles showed mild (< 50%) toxicity at 100 µg/ml, while Ag spheres were not toxic when compared to untreated controls.

AgNPs may also be toxic through the release of Ag ions, so NPs were dispersed (100 µg/ml) in cell culture medium and, after 24 hours of incubation, the particles were removed by centrifugation. NE-4C cells were incubated with particle-free incubation solutions and cell viability assayed after 24 hours incubation. Cell viability was reduced by particle-free supernatants of Ag cubes and triangles but almost no toxicity was observed with the supernatants of spheres or rods (Fig. 4A).

Cellular uptake of AgNPs after 1 hour of incubation was investigated by electron microscopy (Fig. 5). Ag rods resulted in mechanical damage to the cells. The local geometry of silver particles in contact with the cell membrane was important in determining how cells interacted with the microparticles. For example, the sharp edges of rods in contact with the cell membrane allowed the particle to penetrate the cells. This may have been because the sharper contacting geometries made it easier for cells to recruit actin filaments to attach and engulf the objects compared to particles with a round surface. Overall, rod-like and sharp NP geometries made it more likely that they would adhere to and become internalized by the cell. Particles with different shapes in general, and rod-shaped NPs specifically, agglomerate, diffuse, and settle in cell culture medium. Therefore, increased cellular density is also a function of these factors, as it determines the rate of transport of NPs to cells in culture [60].

Electron microscopy failed to demonstrate accumulation of AgNPs in intracellular vesicles and revealed very few particles inside cells, perhaps due to low cellular penetration or the rapid dissolution of particles outside and inside cells.

Discussion

Silver NPs (35–50 nm) exerted shape-dependent toxic effects on neural cells. Toxicity was due to shape-dependent dissolution of Ag ions and the severe mechanical damage caused by rod-shaped NPs. Supporting this, previous studies have shown that NP shape affects the level of cellular toxicity. For instance, amorphous ceramic NPs generated more reactive oxygen species (ROS), the production of which can result in cellular toxicity, than anatase or rutile of the same size. The authors hypothesized that amorphous ceramic NPs had more surface defects and therefore active sites capable of inducing ROS [61]. Another study reported that the anatase form of ceramic NPs were more toxic to neurons than the rutile form, even when synthesized at similar size and chemical composition [62]. Rod-shaped Fe_2O_3 NPs resulted in greater cytotoxicity, lactate dehydrogenase (LDH) release, inflammatory response, ROS production, and necrosis than spheres in murine macrophages (RAW 264.7) [63]. Rod-shaped cerium oxide (CeO_2) NPs were also more toxic than octahedral or cubic particles in terms of LDH and tumor necrosis factor alpha (TNF) release in macrophages [64]. In a previous work, we demonstrated that, the low accumulation of 60nm sized Ag NPs (60 ± 13 nm) in neurovascular blood-brain barrier (NV-BBB) organoids due to its dissolution outside and inside the brain microenvironment [38, 39]. There is therefore

increasing data suggesting that the geometric properties of NPs mediate toxicity, but a more systematic approach would further advance our knowledge with respect to exactly which shapes exert the most cytotoxic effects. Silver NPs are known to exert toxic effects on bacteria, fungi, and mammalian cells. AgNPs were variably toxic due to the variable dissolution of ions, with cubic and triangular NPs releasing more ions than spheres due to dissolution from the sharp edges. In particular, Ag rods showed very high toxicity and increased ion release (results not shown), perhaps due to their shape interacting with cellular membranes. Hence, shape can also influence the interaction between particles and cell membranes, and endocytosis or phagocytosis are influenced by edges and lines on particle surfaces [61, 63–69]

The shape of NPs has previously been shown to be important for mediating the toxic effects of nanomaterials [70, 71]. Indeed, our electron microscopy results showed that Ag nanorods caused severe mechanical cellular injury rather than chemical toxicity. Although there were unexpectedly low number of particles inside NE-4C neural stem cells after one hour of exposure, the few nanorods that were present seemed to completely disrupt the cells. As all AgNPs produce silver ions with their associated kinetics and toxicity effects [72], their wide application as anti-bacterial medical and food packaging additives needs further consideration, particularly with respect to the optimal types and doses of AgNPs that minimize shape-dependent cytotoxicity.

Conclusions

In conclusion, while all shapes of AgNPs adsorbed large amounts of plasma proteins, the amount of adsorption was dependent on the shape. Similarly, cellular toxicity was shape-dependent: rods were highly toxic within an hour of exposure, and cubes and triangles were toxic at high concentrations after 24 hours. While rods presumably mediated their toxicity via mechanical damage, the shape might also result in the rapid release of Ag ions and indirect cytotoxicity.

Declarations

Funding This study was supported by the EU FP7 Marie Curie Actions, Network for Initial Training NanoTOES (PITN-GA-2010-264506).

Conflicts of interest/Competing interests The authors declare no competing interests

References

1. Vance ME, Kuiken T, Vejerano EP, McGinnis SP, Hochella MF Jr, Rejeski D et al (2015) Nanotechnology in the real world: Redeveloping the nanomaterial consumer products inventory. Beilstein J Nanotechnol 6:1769–1780
2. Morris D, Ansar M, Speshock J, Ivanciuc T, Qu Y, Casola A et al. Antiviral and Immunomodulatory Activity of Silver Nanoparticles in Experimental RSV Infection. Viruses. 2019;11(8)

3. Thi Ngoc Dung T, Nang Nam V, Thi Nhan T, Ngoc TTB, Minh LQ, Nga BTT et al (2020) Silver nanoparticles as potential antiviral agents against African swine fever virus. Materials Research Express 6(12):1250g9
4. Yang XX, Li CM, Huang CZ (2016) Curcumin modified silver nanoparticles for highly efficient inhibition of respiratory syncytial virus infection. Nanoscale 8(5):3040–3048
5. Genter MB, Newman NC, Shertzer HG, Ali SF, Bolon B (2012) Distribution and systemic effects of intranasally administered 25 nm silver nanoparticles in adult mice. Toxicol Pathol 40(7):1004–1013
6. Patchin ES, Anderson DS, Silva RM, Uyeminami DL, Scott GM, Guo T et al (2016) Size-Dependent Deposition, Translocation, and Microglial Activation of Inhaled Silver Nanoparticles in the Rodent Nose and Brain. Environ Health Perspect 124(12):1870–1875
7. Garcia GJ, Schroeter JD, Kimbell JS (2015) Olfactory deposition of inhaled nanoparticles in humans. Inhalation toxicology 27(8):394–403
8. Kovács T (2004) Mechanisms of olfactory dysfunction in aging and neurodegenerative disorders. Ageing Res Rev 3(2):215–232
9. Tian L, Shang Y, Chen R, Bai R, Chen C, Inthavong K et al (2019) Correlation of regional deposition dosage for inhaled nanoparticles in human and rat olfactory. Part Fibre Toxicol 16(1):6
10. Oberdorster G, Elder A, Rinderknecht A (2009) Nanoparticles and the brain: cause for concern? J Nanosci Nanotechnol 9(8):4996–5007
11. Oberdörster G, Sharp Z, Atudorei V, Elder A, Gelein R, Kreyling W et al (2004) Translocation of inhaled ultrafine particles to the brain. Inhalation toxicology 16(6–7):437–445
12. Wang B, Feng WY, Wang M, Shi JW, Zhang F, Ouyang H et al (2007) Transport of intranasally instilled fine Fe2O3 particles into the brain: micro-distribution, chemical states, and histopathological observation. Biol Trace Elem Res 118(3):233–243
13. Illum L (2000) Transport of drugs from the nasal cavity to the central nervous system. Eur J Pharm Sci 11(1):1–18
14. Aschner M (2009) Chapter 8 - Nanoparticles: Transport across the olfactory epithelium and application to the assessment of brain function in health and disease. Prog Brain Res 180:141–152
15. De Lorenzo AJ. Electron microscopy of the olfactory and gustatory pathways. The Annals of otology, rhinology, and laryngology. 1960;69:410–20
16. Elder A, Gelein R, Silva V, Feikert T, Opanashuk L, Carter J et al (2006) Translocation of inhaled ultrafine manganese oxide particles to the central nervous system. Environ Health Perspect 114(8):1172–1178
17. Hopkins LE, Patchin ES, Chiu PL, Brandenberger C, Smiley-Jewell S, Pinkerton KE (2014) Nose-to-brain transport of aerosolised quantum dots following acute exposure. Nanotoxicology 8(8):885–893
18. Mistry A, Stolnik S, Illum L (2009) Nanoparticles for direct nose-to-brain delivery of drugs. Int J Pharm 379(1):146–157

19. Patel S, Chavhan S, Soni H, Babbar AK, Mathur R, Mishra AK et al (2011) Brain targeting of risperidone-loaded solid lipid nanoparticles by intranasal route. J Drug Target 19(6):468–474
20. Dan M, Wen H, Shao A, Xu L (2018) Silver Nanoparticle Exposure Induces Neurotoxicity in the Rat Hippocampus Without Increasing the Blood-Brain Barrier Permeability. J Biomed Nanotechnol 14(7):1330–1338
21. Sharma HS, Ali SF, Hussain SM, Schlager JJ, Sharma A (2009) Influence of engineered nanoparticles from metals on the blood-brain barrier permeability, cerebral blood flow, brain edema and neurotoxicity. An experimental study in the rat and mice using biochemical and morphological approaches. J Nanosci Nanotechnol 9(8):5055–5072
22. Kalishwaralal K, Banumathi E, Ram Kumar Pandian S, Deepak V, Muniyandi J, Eom SH et al (2009) Silver nanoparticles inhibit VEGF induced cell proliferation and migration in bovine retinal endothelial cells. Colloids surfaces B Biointerfaces 73(1):51–57
23. Trickler WJ, Lantz-McPeak SM, Robinson BL, Paule MG, Slikker W Jr, Biris AS et al (2014) Porcine brain microvessel endothelial cells show pro-inflammatory response to the size and composition of metallic nanoparticles. Drug Metab Rev 46(2):224–231
24. Shannahan JH, Podila R, Aldossari AA, Emerson H, Powell BA, Ke PC et al (2015) Formation of a protein corona on silver nanoparticles mediates cellular toxicity via scavenger receptors. Toxicol Sci 143(1):136–146
25. De Matteis V, Malvindi MA, Galeone A, Brunetti V, De Luca E, Kote S et al (2015) Negligible particle-specific toxicity mechanism of silver nanoparticles: the role of Ag + ion release in the cytosol. Nanomedicine: nanotechnology biology medicine 11(3):731–739
26. Stoehr LC, Gonzalez E, Stampfl A, Casals E, Duschl A, Puntes V et al (2011) Shape matters: effects of silver nanospheres and wires on human alveolar epithelial cells. Part Fibre Toxicol 8:36
27. Asharani PV, Hande MP, Valiyaveettil S (2009) Anti-proliferative activity of silver nanoparticles. BMC Cell Biol 10:65
28. Urbanska K, Pajak B, Orzechowski A, Sokolowska J, Grodzik M, Sawosz E et al (2015) The effect of silver nanoparticles (AgNPs) on proliferation and apoptosis of in ovo cultured glioblastoma multiforme (GBM) cells. Nanoscale Res Lett 10:98
29. Luther EM, Koehler Y, Diendorf J, Epple M, Dringen R (2011) Accumulation of silver nanoparticles by cultured primary brain astrocytes. Nanotechnology 22(37):375101
30. Soderstjerna E, Johansson F, Klefbohm B, Englund Johansson U (2013) Gold- and silver nanoparticles affect the growth characteristics of human embryonic neural precursor cells. PLoS One 8(3):e58211
31. Xu F, Piett C, Farkas S, Qazzaz M, Syed NI (2013) Silver nanoparticles (AgNPs) cause degeneration of cytoskeleton and disrupt synaptic machinery of cultured cortical neurons. Mol Brain 6:29
32. Repar N, Li H, Aguilar JS, Li QQ, Drobne D, Hong Y (2018) Silver nanoparticles induce neurotoxicity in a human embryonic stem cell-derived neuron and astrocyte network. Nanotoxicology 12(2):104–116

33. Madathiparambil Visalakshan R, Gonzalez Garcia LE, Benzigar MR, Ghazaryan A, Simon J, Mierczynska-Vasilev A et al (2020) The Influence of Nanoparticle Shape on Protein Corona Formation. Small 16(25):e2000285
34. Cho EC, Au L, Zhang Q, Xia Y (2010) The effects of size, shape, and surface functional group of gold nanostructures on their adsorption and internalization by cells. Small 6(4):517–522
35. Kumarasamy M, Sosnik A (2019) The Nose-To-Brain Transport of Polymeric Nanoparticles Is Mediated by Immune Sentinels and Not by Olfactory Sensory Neurons. Advanced Biosystems 3(12):1900123
36. Murali K, Kenesei K, Li Y, Demeter K, Környei Z, Madarász E (2015) Uptake and bio-reactivity of polystyrene nanoparticles is affected by surface modifications, ageing and LPS adsorption: in vitro studies on neural tissue cells. Nanoscale 7(9):4199–4210
37. Izak-Nau E, Kenesei K, Murali K, Voetz M, Eiden S, Puntes VF et al (2014) Interaction of differently functionalized fluorescent silica nanoparticles with neural stem- and tissue-type cells. Nanotoxicology 8(Suppl 1):138–148
38. Kumarasamy M, Sosnik A. Multicellular Organoids of the Neurovascular Blood-Brain Barrier: A New Platform for Precision Neuronanomedicine. bioRxiv. 2020:2020.08.14.249326
39. Kumarasamy M, Sosnik A. Heterocellular Spheroids of the Neurovascular Blood-Brain Barrier as A Platform for Personalized Nanoneuromedicine. iScience. 2021:102183
40. Qi X, Balankura T, Zhou Y, Fichthorn KA (2015) How Structure-Directing Agents Control Nanocrystal Shape: Polyvinylpyrrolidone-Mediated Growth of Ag Nanocubes. Nano Lett 15(11):7711–7717
41. Safo IA, Werheid M, Dosche C, Oezaslan M (2019) The role of polyvinylpyrrolidone (PVP) as a capping and structure-directing agent in the formation of Pt nanocubes. Nanoscale Advances 1(8):3095–3106
42. Song YJ, Wang M, Zhang XY, Wu JY, Zhang T (2014) Investigation on the role of the molecular weight of polyvinyl pyrrolidone in the shape control of high-yield silver nanospheres and nanowires. Nanoscale Res Lett 9(1):17
43. Bastús NG, Merkoçi F, Piella J, Puntes V (2014) Synthesis of Highly Monodisperse Citrate-Stabilized Silver Nanoparticles of up to 200 nm: Kinetic Control and Catalytic Properties. Chem Mater 26(9):2836–2846
44. Zhang Q, Li W, Wen LP, Chen J, Xia Y (2010) Facile synthesis of Ag nanocubes of 30 to 70 nm in edge length with CF(3)COOAg as a precursor. Chemistry 16(33):10234–10239
45. Zhang Q, Li N, Goebl J, Lu Z, Yin Y (2011) A systematic study of the synthesis of silver nanoplates: is citrate a "magic". reagent? J Am Chem Soc 133(46):18931–18939
46. Rai AJ, Gelfand CA, Haywood BC, Warunek DJ, Yi J, Schuchard MD et al (2005) HUPO Plasma Proteome Project specimen collection and handling: towards the standardization of parameters for plasma proteome samples. Proteomics 5(13):3262–3277
47. Schlett K, Madarasz E (1997) Retinoic acid induced neural differentiation in a neuroectodermal cell line immortalized by p53 deficiency. J Neurosci Res 47(4):405–415

48. Mosmann T (1983) Rapid colorimetric assay for cellular growth and survival: application to proliferation and cytotoxicity assays. J Immunol Methods 65(1–2):55–63
49. Sun Y, Xia Y (2002) Shape-controlled synthesis of gold and silver nanoparticles. Science 298(5601):2176–2179
50. Wiley B, Sun Y, Mayers B, Xia Y (2005) Shape-controlled synthesis of metal nanostructures: the case of silver. Chemistry 11(2):454–463
51. Khan I, Saeed K, Khan I. Nanoparticles (2019) Properties, applications and toxicities. Arabian Journal of Chemistry 12(7):908–931
52. Kumar CSSR, Jing H. UV-VIS and photoluminescence spectroscopy for nanomaterials characterization. Berlin; New York: Springer Reference; 2013. xii, 599 pages p
53. Li C, Sun L, Sun Y, Teranishi T (2013) One-Pot Controllable Synthesis of Au@Ag Heterogeneous Nanorods with Highly Tunable Plasmonic Absorption. Chem Mater 25(13):2580–2590
54. Sun Y, Gates B, Mayers B, Xia Y (2002) Crystalline Silver Nanowires by Soft Solution Processing. Nano Lett 2(2):165–168
55. Sun Y, Xia Y (2002) Large-Scale Synthesis of Uniform Silver Nanowires Through a Soft, Self-Seeding, Polyol Process. Adv Mater 14(11):833–837
56. Sun Y, Mayers B, Herricks T, Xia Y (2003) Polyol Synthesis of Uniform Silver Nanowires: A Plausible Growth Mechanism and the Supporting Evidence. Nano Lett 3(7):955–960
57. Vroman L, Adams AL, Fischer GC, Munoz PC (1980) Interaction of high molecular weight kininogen, factor XII, and fibrinogen in plasma at interfaces. Blood 55(1):156–159
58. Gagner JE, Lopez MD, Dordick JS, Siegel RW (2011) Effect of gold nanoparticle morphology on adsorbed protein structure and function. Biomaterials 32(29):7241–7252
59. Ferdous Z, Nemmar A (2020) Health Impact of Silver Nanoparticles: A Review of the Biodistribution and Toxicity Following Various Routes of Exposure. Int J Mol Sci 21(7):2375
60. Teeguarden JG, Hinderliter PM, Orr G, Thrall BD, Pounds JG (2007) Particokinetics in vitro: dosimetry considerations for in vitro nanoparticle toxicity assessments. Toxicol Sci 95(2):300–312
61. Jiang J, Oberdörster G, Elder A, Gelein R, Mercer P, Biswas P (2008) Does Nanoparticle Activity Depend upon Size Crystal Phase? Nanotoxicology 2(1):33–42
62. Wu J, Sun J, Xue Y (2010) Involvement of JNK and P53 activation in G2/M cell cycle arrest and apoptosis induced by titanium dioxide nanoparticles in neuron cells. Toxicology letters 199(3):269–276
63. Lee JH, Ju JE, Kim BI, Pak PJ, Choi EK, Lee HS et al (2014) Rod-shaped iron oxide nanoparticles are more toxic than sphere-shaped nanoparticles to murine macrophage cells. Environmental toxicology chemistry 33(12):2759–2766
64. Forest V, Leclerc L, Hochepied JF, Trouvé A, Sarry G, Pourchez J (2017) Impact of cerium oxide nanoparticles shape on their in vitro cellular toxicity. Toxicology in vitro: an international journal published in association with BIBRA 38:136–141

65. He Y, Park K (2016) Effects of the Microparticle Shape on Cellular Uptake. Mol Pharm 13(7):2164–2171
66. Huang C, Zhang Y, Yuan H, Gao H, Zhang S (2013) Role of nanoparticle geometry in endocytosis: laying down to stand up. Nano Lett 13(9):4546–4550
67. Oh N, Park JH (2014) Endocytosis and exocytosis of nanoparticles in mammalian cells. Int J Nanomedicine 9(Suppl 1(Suppl 1):51–63
68. Salatin S, Maleki Dizaj S, Yari Khosroushahi A (2015) Effect of the surface modification, size, and shape on cellular uptake of nanoparticles. Cell Biol Int 39(8):881–890
69. Xie X, Liao J, Shao X, Li Q, Lin Y (2017) The Effect of shape on Cellular Uptake of Gold Nanoparticles in the forms of Stars, Rods, and Triangles. Sci Rep 7(1):3827
70. Dong L, Tang S, Deng F, Gong Y, Zhao K, Zhou J et al (2019) Shape-dependent toxicity of alumina nanoparticles in rat astrocytes. Sci Total Environ 690:158–166
71. Allegri M, Bianchi MG, Chiu M, Varet J, Costa AL, Ortelli S et al (2016) Shape-Related Toxicity of Titanium Dioxide Nanofibres. PLoS One 11(3):e0151365
72. Smith JN, Thomas DG, Jolley H, Kodali VK, Littke MH, Munusamy P et al (2018) All that is silver is not toxic: silver ion and particle kinetics reveals the role of silver ion aging and dosimetry on the toxicity of silver nanoparticles. Part Fibre Toxicol 15(1):47

Figures

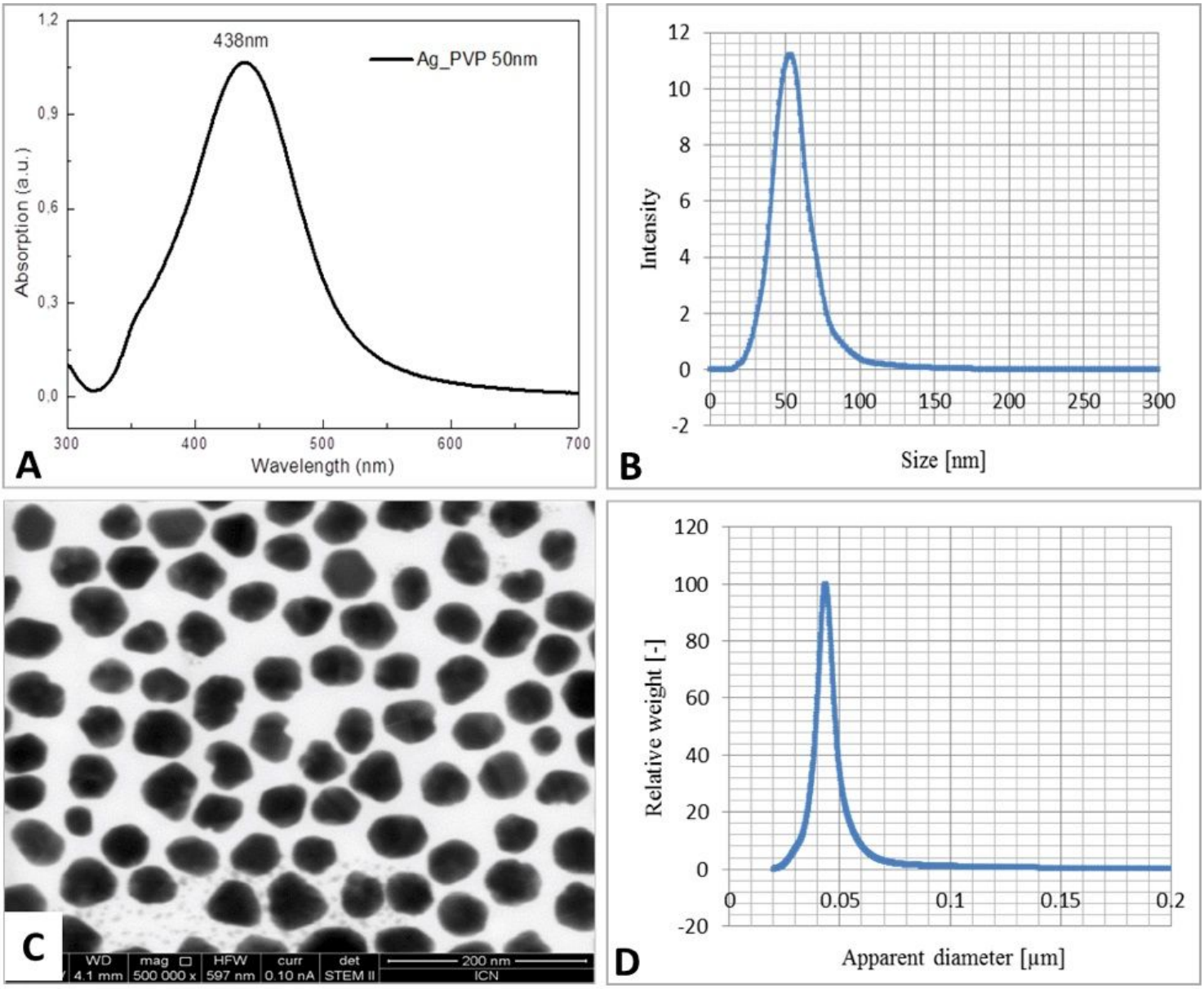

Figure 1

Shape and monodispersity of 50 nm spherical AgNPs by (A) UV-vis spectroscopy, (B) NTA, (C) TEM, (D) DCS.

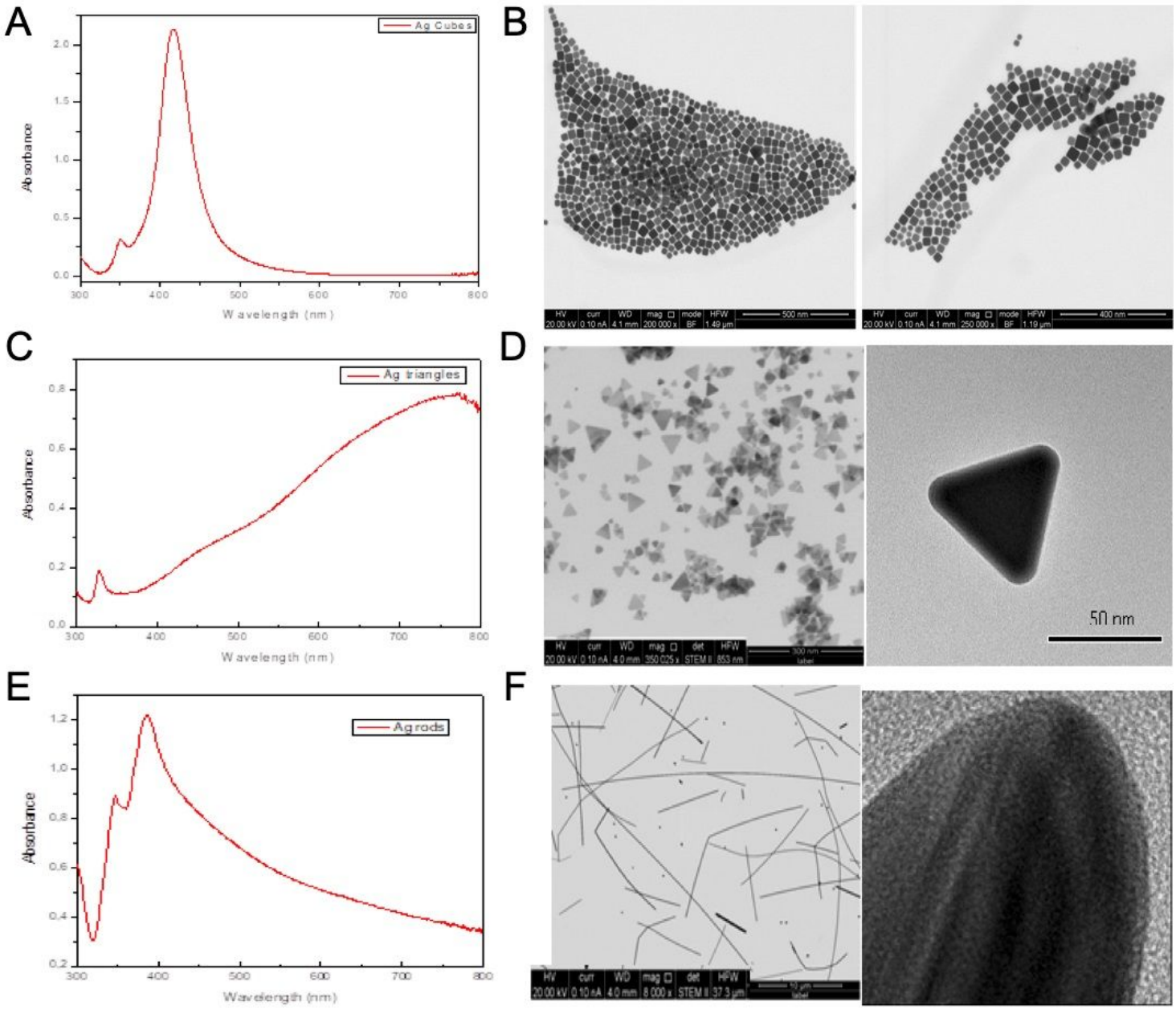

Figure 2

(A) UV-vis absorption spectrum of the aqueous solution of silver nanocubes with edge lengths of 35-45 nm. (B) TEM images of Ag nanocubes obtained by a standard polyol synthesis. (C) UV-vis absorption spectrum of the aqueous solution of Ag nanotriangles/platelets. (D) TEM and HR-TEM images of Ag nanotriangles/plates. By TEM, the synthesized product was triangular with edge lengths of 31.5 ± 11 nm and platelet thickness of 4.5 ± 0.9 nm. (E) UV-vis absorption spectrum of the aqueous solutions of silver nanorods. (F) TEM and HR-TEM images of Ag nanorods.

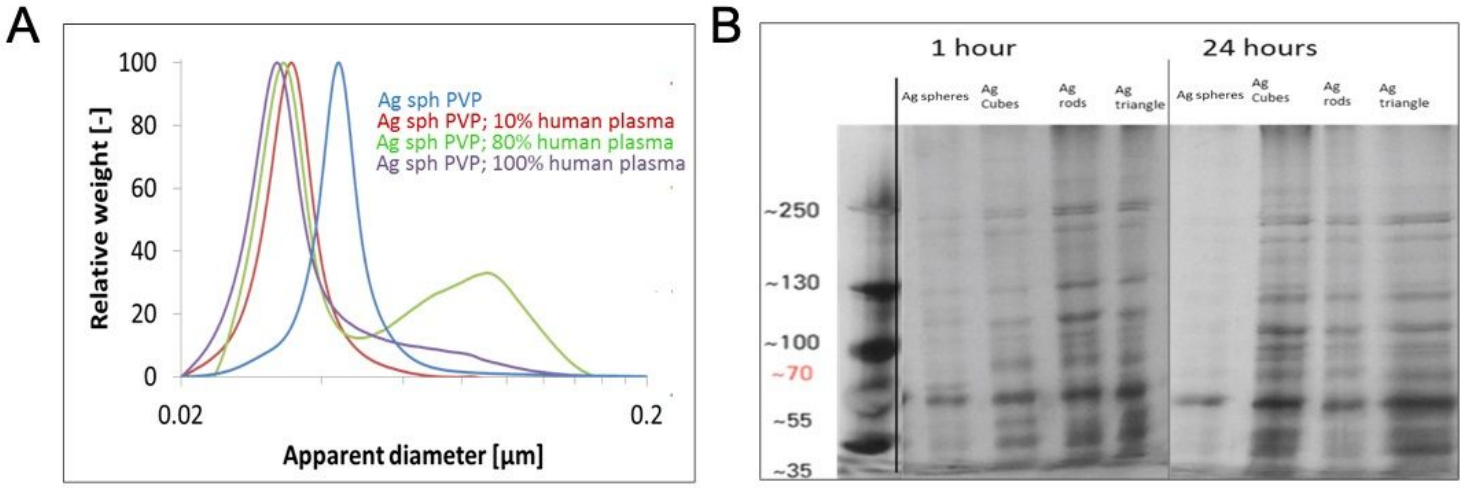

Figure 3

(A) DCS measurements of AgNP-corona complexes before and after incubation with plasma. (B) SDS-PAGE of the protein coronas of different forms of AgNPs incubated in 100% human plasma for 1 h and 24 h.

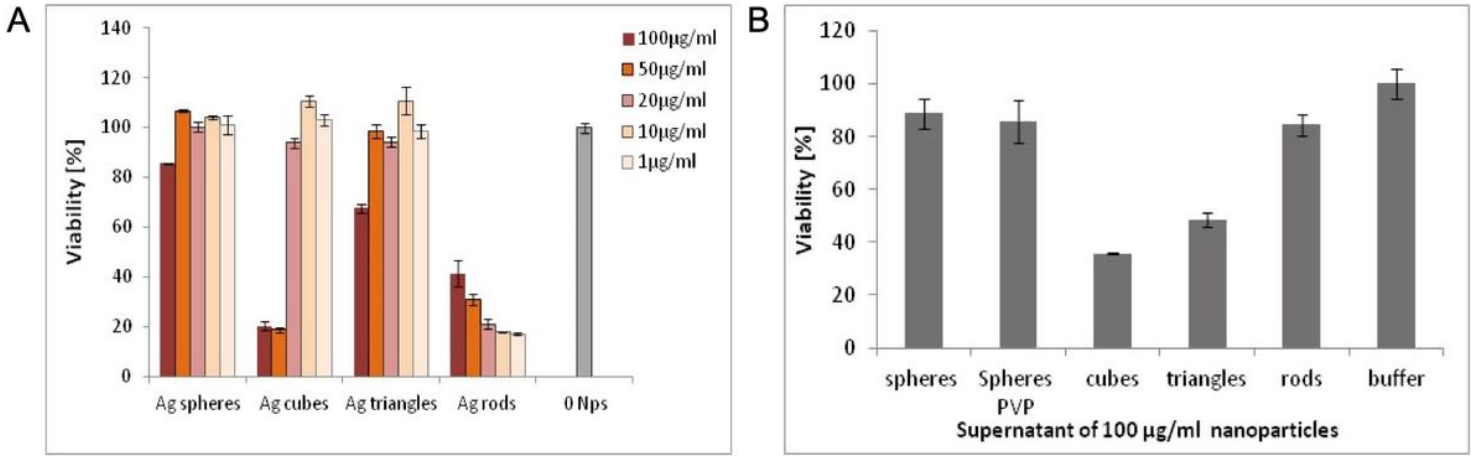

Figure 4

(A) Shape-dependent effects of AgNPs on the metabolic activity of NE-4C neural stem cells (MTT assay). (B) The effects of particle-free supernatants of NP suspensions on the viability of NE-4C cells. Spheres PVP: Ag spheres kept in PVP-containing buffer prior to dispersion in the culture medium.

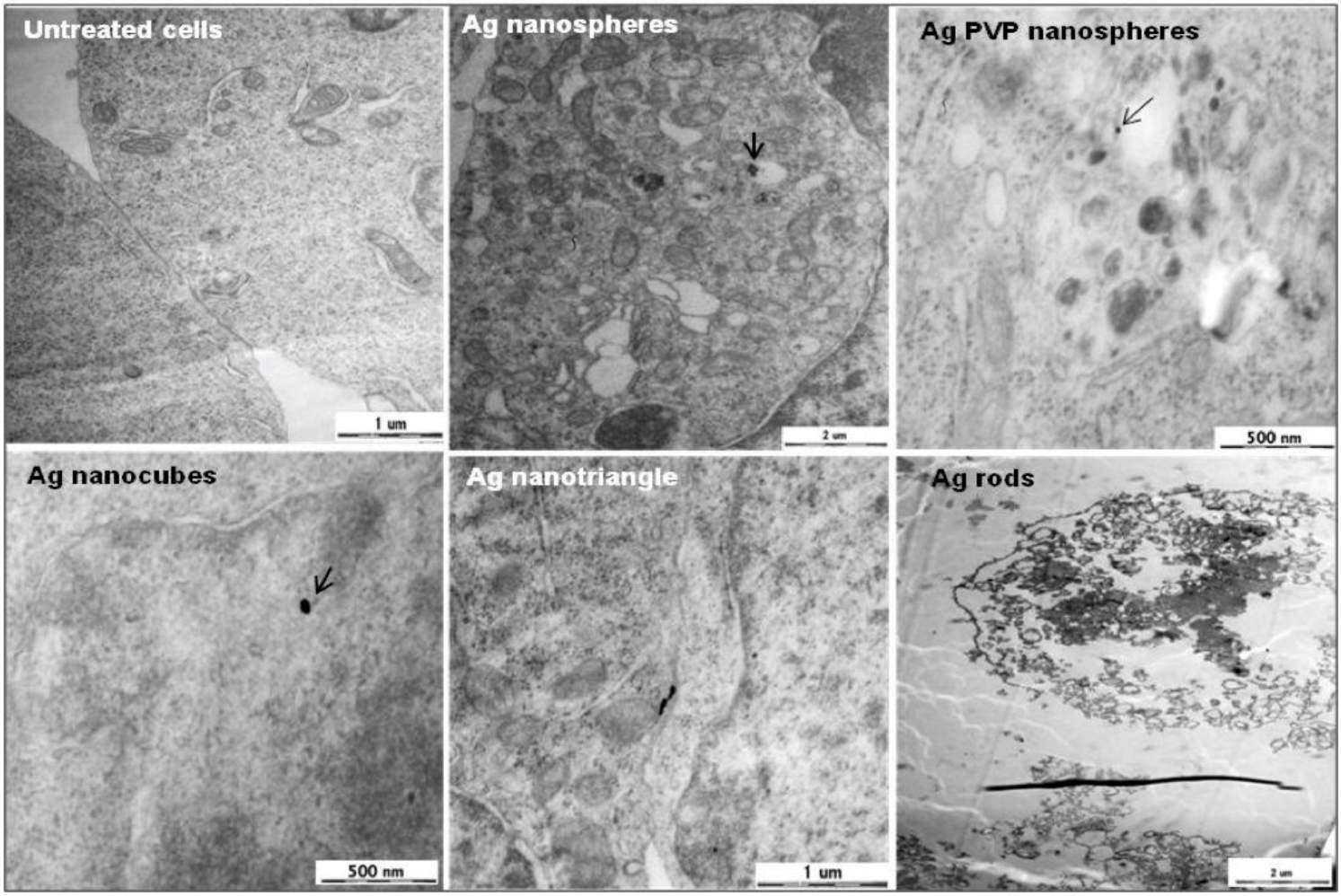

Figure 5

Spherical, cubical, or triangular AgNPs did not cause severe structural damage to NE-4C cells after one hour of exposure. By contrast, NE-4C cells were disrupted by Ag nanorods.

Supplementary Files

This is a list of supplementary files associated with this preprint. Click to download.

- GraphicalAbstract.jpg